vide an unbiased sample of hubs from the point of view of in- and out-connectivity, half of those nodes were selected as the highest out-degree hubs (8 baits with $K_{bait} \geq 90$ for the interaction network and 7 nodes with $K_{out} \geq 34$ for the regulatory network), while half were the highest in-degree hubs (7 preys with $K_{prey} \geq 20$ for the interaction network and 8 nodes with $K_{out} \geq 8$ for the regulatory network). In agreement with the correlation properties described above, direct connections between hubs were significantly suppressed. In the interaction network, we observed 20 links between different hubs in this group, which is significantly below 56 ± 7.5 links in the randomized network. In the transcription regulatory network, there were 16 links between hubs in real network, as opposed to 35 ± 6.5 in its randomized version. Not only are direct links between hubs suppressed in both studied networks, but hubs also tend to share fewer of their neighbors with other hubs, thereby extending their isolation to the level of next-nearest neighbor connections. The total number of paths of length 2 between the set of 15 hubs in the interaction network is equal to 418, whereas in the null model we measured this number to be 653 ± 56. Similarly, for the transcriptional network the number of paths of length 2 is equal to 186 in the real network, whereas from the null model one expects it to be 262 ± 30. Since the number of paths of length 2 between a pair of proteins is equal to the number of their common interaction partners, one concludes that both the hub node itself and its immediate surroundings tend to separate from other hubs, reinforcing the picture of functional modules clustered around individual hubs.

A further implication of the observed correlation is in the suppression of the propagation of deleterious perturbations over the network. It is reasonable to assume that certain perturbations such as, e.g., significant changes in the concentration of a given protein (including its vanishing altogether in a null-mutant cell) with a ceratin probability can affect its first, second, and sometimes even more distant neighbors in the corresponding network. While the number of immediate neighbors of a node is by definition equal to its own connectivity K_0, the average number of its second neighbors, given by $K_0 \langle (K_1 - 1) \rangle_{K0}$, is sensitive to correlation patterns of the network. Because highly connected nodes serve as powerful amplifiers for the propagation of deleterious perturbations, it is especially important to suppress this propagation beyond their immediate neighbors. It was argued that scale-free networks in general are very vulnerable to attacks aimed at highly connected nodes (*12, 13*). The anticorrelation presented above implies a reduced branching ratio around these nodes and thus provides a certain degree of protection against such attacks. This may be the reason why the correlation between the connectivity of a given protein and the lethality of the mutant cell lacking this protein is not particularly strong (*8*).

It is feasible that molecular networks in a living cell have organized themselves in an interaction pattern that is both robust and specific. Topologically, the specificity of different functional modules can be enhanced by limiting interactions between hubs and suppressing the average connectivity of their neighbors. We have seen that such a correlation pattern appears in a similar way in two different layers of molecular networks in yeast, and thus presumably is a universal feature of all molecular networks operating in living cells.

References and Notes

1. P. Uetz *et al.*, *Nature* **403**, 623 (2000).
2. T. Ito *et al.*, *Proc. Natl. Acad. Sci. U.S.A.* **98**, 4569 (2001).
3. M. C. Costanzo *et al.*, *Nucleic Acids Res.* **29**, 75 (2001).
4. A. L. Barabási, R. Albert, *Science* **286**, 509 (1999).
5. A. Broder *et al.*, *Comput. Networks* **33**, 309 (2000).
6. H. Jeong, B. Tombor, R. Albert, Z. N. Oltvai, A.-L. Barabási, *Nature* **407**, 651 (2000); D. A. Fell, A. Wagner, *Nature Biotechnol.* **18**, 1121 (2000).
7. A. Wagner, *Mol. Biol. Evol.* **18**, 1283 (2001).
8. H. Jeong, S. Mason, A.-L. Barabasi, Z. N. Oltvai, *Nature* **411**, 41 (2001).
9. A.-C. Gavin *et al.*, *Nature* **415**, 141 (2002).
10. R. Pastor-Satorras, A. Vazquez, A. Vespignani, *Phys. Rev. Lett.* **87**, 258701 (2001).
11. L. H. Hartwell, J. J. Hopfield, S. Leibler, A. W. Murray, *Nature* **402** (6761 suppl.), C47 (1999).
12. R. Albert, H. Jeong, A.-L. Barabasi, *Nature* **406**, 378 (2000).
13. B. Vogelstein, D. Lane, A. J. Levine, *Nature* **408**, 307 (2000).

14. Supported in part by the NSF under grant PHY99-07949. Work at Brookhaven National Laboratory was carried out under Contract No. DE-AC02-98CH10886, Division of Material Science, U.S. Department of Energy. We thank the Institute for Theoretical Physics at the University of California at Santa Barbara, Nordita, and the University of Tokyo (for S.M.) for hospitality, K. Eriksen for valuable comments on the manuscript, T. Hwa for suggesting the subject of two-hybrid experiments, and T. Ito for providing the information on limitations of his experimental techniques.

6 August 2001; accepted 25 March 2002

Partitioning of Lipid-Modified Monomeric GFPs into Membrane Microdomains of Live Cells

David A. Zacharias,[1,3*†] Jonathan D. Violin,[1,2*] Alexandra C. Newton,[1] Roger Y. Tsien[1,3‡]

Many proteins associated with the plasma membrane are known to partition into submicroscopic sphingolipid- and cholesterol-rich domains called lipid rafts, but the determinants dictating this segregation of proteins in the membrane are poorly understood. We suppressed the tendency of *Aequorea* fluorescent proteins to dimerize and targeted these variants to the plasma membrane using several different types of lipid anchors. Fluorescence resonance energy transfer measurements in living cells revealed that acyl but not prenyl modifications promote clustering in lipid rafts. Thus the nature of the lipid anchor on a protein is sufficient to determine submicroscopic localization within the plasma membrane.

Subcellular compartmentalization of signaling increases the specificity and efficiency of signal transduction. Caveolae and lipid rafts are related microdomains of the plasma membrane that are enriched in cholesterol, sphingolipids, and many signaling proteins (*1, 2*). Whereas protein-protein interactions maintain many signaling complexes (*3, 4*), specific lipid modifications are believed sufficient to sequester proteins in lipid rafts and caveolae. In particular, acylated proteins may preferentially partition into these compartments (*5, 6*). Unambiguous observation of these small (<100-nm) microdomains in living cells is beyond the resolution of visible light microscopy; thus destructive assays such as cellular fractionation (*7*) or immunolocalization by electron microscopy (*8*) have been relied upon to study lipid rafts and caveolae. We now use fluorescence resonance energy transfer (FRET) between nondimerizing cyan (CFP) and yellow (YFP) variants of *Aequorea* green fluorescent protein (*9, 10*) to show which lipid modifications are sufficient to cause such test proteins to aggregate within lipid rafts inside living cells. FRET from CFP to YFP is advantageous, because it nondestructively detects proximities at nanometer

[1]Department of Pharmacology, [2]Biomedical Sciences Graduate Program, and [3]Howard Hughes Medical Institute, University of California, San Diego, La Jolla, CA 92093–0647, USA.

*These authors contributed equally to this work.
†Present address: Merck Research Laboratories, 3535 General Atomics Court, MRLSDB1, San Diego, CA 92121, USA.
‡To whom correspondence should be addressed. E-mail: rtsien@ucsd.edu

scales and because CFP and YFP have no targeting signals aside from the lipid anchors we added.

We fused CFP and YFP onto short peptides containing consensus sequences for acylation (*11*) or prenylation (*12*) (Fig. 1A). These constructs (*13*) were transfected with Lipofectin (GibcoBRL) into Madin-Darby canine kidney (MDCK) cells, and the cells were imaged at 80 to 90% confluency. Regions of interest were chosen from plasmalemmal sites where there was obvious cell-cell contact and little or no interference from fluorescence from intracellular membranes (Fig. 1B). The associative properties of coexpressed lipid-modified CFP and YFP pairs were determined by measuring the FRET efficiency (FRET E%) and fitting those values to the simplest possible saturable binding model, in which E% is a hyperbolic function of the surface density or local fluorescence intensity F of the acceptor, YFP.

$$E\% = \frac{E\%_{max}F}{F + K} \quad (1)$$

We preferred such a saturable isotherm over a linear fit with adjustable slope and intercept because the hyperbola also has two free parameters yet intrinsically satisfies the physical constraints that E% must approach zero as F approaches zero and that E% must level off no matter how much acceptor is expressed. Also, the parameter K is analogous to a dissociation constant and provides a natural criterion for the degree of clustering at any given concentration of acceptor (illustrated in Fig. 2). When $F \ll K$, FRET efficiencies are approximately proportional to acceptor surface densities, because the donors and acceptors are mutually randomly distributed. When $F \gg K$, FRET efficiencies are nearly saturated and independent of further increases in acceptor density (*14*), because each donor is already clustered with at least one acceptor. FRET E% was determined by selectively photobleaching the acceptor YFP and measuring the resulting increase in brightness of CFP emission as a percentage of the final CFP intensity (*15*).

Myristoyl and palmitoyl chains were attached to CFP and YFP by genetically fusing an acylation substrate sequence from the 13 NH_2-terminal residues of the kinase Lyn to the NH_2-termini of the fluorescent proteins. FRET efficiencies in regions of interest (ROIs) of cells expressing these constructs (MyrPalm-CFP and -YFP) showed that E% was saturated, indicating strong clustering (Fig. 3A). However, this clustered distribution survived extraction with 10 mM 5-methyl-β-cyclodextrin (MβCD) (Fig. 3B), a treatment known to disrupt lipid rafts and caveolae by depletion of cholesterol (*16*).

We suspected the residual clustering to be an artifact of the known tendency of all forms of GFP to dimerize at high concentrations, which would be particularly likely for proteins confined to two dimensions. To determine accurately the degree to which GFPs interact, we measured the homoaffinity of purified recombinant YFP (not membrane-anchored) by sedimentation equilibrium analytical ultracentrifugation (*15*, *17*) and found a K_d of 0.11 mM (Fig. 4, A and C) (*18*). We replaced hydrophobic residues at the crystallographic interface of the dimer (*19*) with positively charged residues (A206K, L221K, or F223R) (*15*). These mutants were likewise expressed and purified, and their self-association was measured by analytical ultracentrifugation. YFP homoaffinity was reduced to the point that dimerization was essentially eliminated (Fig. 4, B and D, and Table 1). We call these novel monomeric GFP variants mCFP, mGFP, and mYFP. These mutations caused no significant alterations in the spectral properties. When the NH_2-terminus of Lyn was fused to mCFP and mYFP to cause

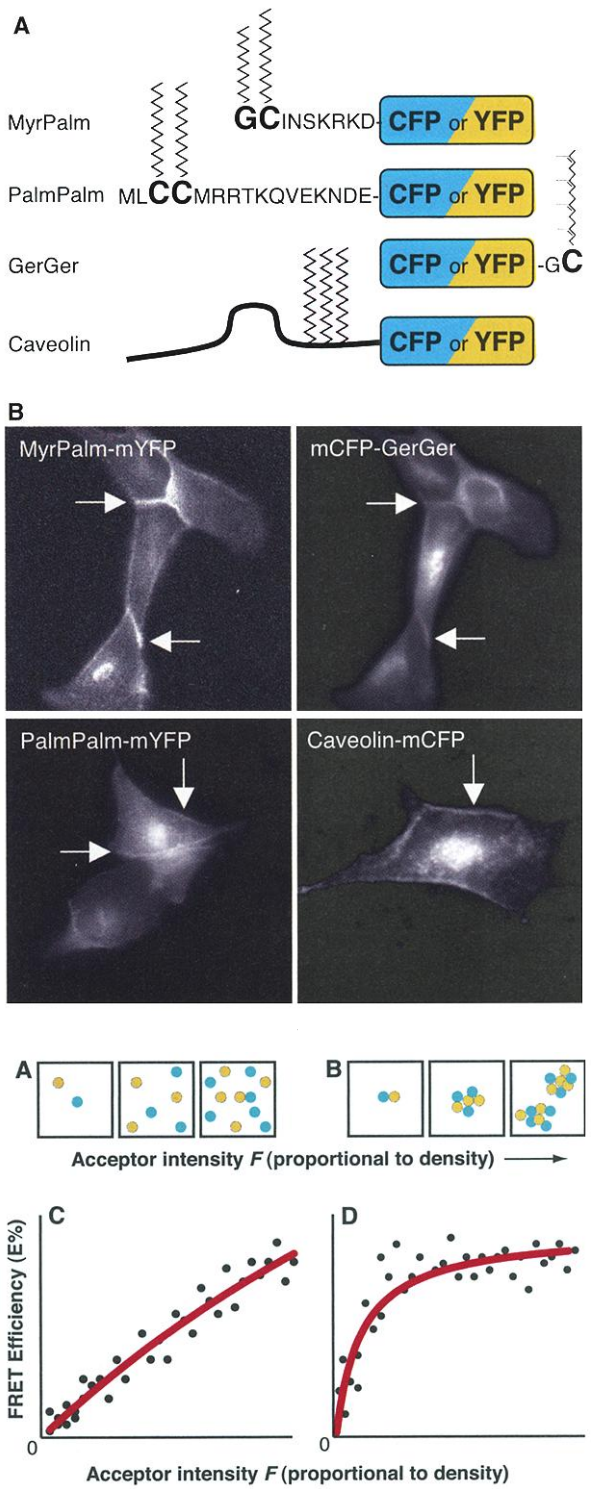

Fig. 1. Lipid-modified fluorescent proteins used in this work and representative images of their expression in MDCK cells. (**A**) MyrPalm (myristoylated and palmitoylated), GerGer (geranylgeranylated), PalmPalm (tandemly palmitoylated), and caveolin (full-length bovine caveolin-1, triply palmitoylated with a putative membrane-embedded hairpin loop) fusion constructs were generated by polymerase chain reaction primer extension. Lipid attachment sites are shown in bold. (**B**) Typical fluorescence images of MDCK cells expressing each construct. Arrows denote representative sites for defining regions for data collection, on membrane sites of cell-cell contact remote from intracellular membranes. mCFP-GerGer and MyrPalm-mYFP images were taken from the same cells.

Fig. 2. Theoretical expectations for unclustered (**A** and **C**) versus clustered (**B** and **D**) donors and acceptors (cyan and yellow circles representing mCFP and mYFP) in a region of interest of a cell membrane (black boxes).

myristoylation and palmitoylation, the proteins were clustered (Fig. 3C), but this clustering was destroyed by MβCD (Fig. 3D, showing *E*% nearly linearly proportional to *F*, i.e., $F \ll K$ in Eq. 1). The latter result showed that the antidimerization mutations and MβCD extraction procedure were effective and that the clustering seen in unperturbed cells could now be attributed to lipid partitioning into microdomains rather than CFP-YFP affinity. mCFP and mYFP were used for all subsequent experiments. It is noteworthy that the visible distribution of MyrPalm-GFPs to plasma membranes was similar with or without MβCD, indicating the utility of FRET for discrimination and analysis of submicron-size domains of plasma membrane. These data also suggest that the domains must be fairly small, as larger domains would cause intradomain, density-dependent FRET, and no clustering would be seen.

We next measured the associations of various lipid modifications with caveolin, a marker for caveolae, a type of lipid raft. MyrPalm-mYFP clustered with full-length caveolin-1 fused to mCFP (Fig. 3E), and MyrPalm-mCFP likewise clustered with caveolin-1–mYFP. mYFP fused to the NH_2-terminal 20 residues of GAP-43 to cause dual palmitoylation (PalmPalm-mYFP) and was also clustered with caveolin-1–mCFP (Fig. 3F). Thus, acylation by fatty acids suffices to cause clustering of test fluorescent proteins in lipid rafts and caveolae.

To examine the effectiveness of prenyl adducts in causing clustering, we fused the CAAX box (*12*) from the guanosine triphosphatase Rho to the COOH-terminus of mCFP and mYFP to cause the addition of a single geranylgeranyl group (mCFP-GerGer and mYFP-GerGer). These constructs clustered with each other (Fig. 3G), even after extraction of cholesterol with 10 mM MβCD (Fig. 3H). However, mYFP-GerGer did not cluster with caveolin-1–mCFP (Fig. 3I), nor did mCFP-GerGer congregate with MyrPalm-mYFP (Fig. 3J), suggesting that geranylgeranylation promotes clustering but not in cholesterol- and sphingolipid-rich lipid rafts.

We also used traditional biochemical methods to examine partitioning of lipid-modified YFPs into detergent-soluble or detergent-insoluble membranes, or into low- or high-density membranes after carbonate extraction (*15*). These techniques confirmed the results of the

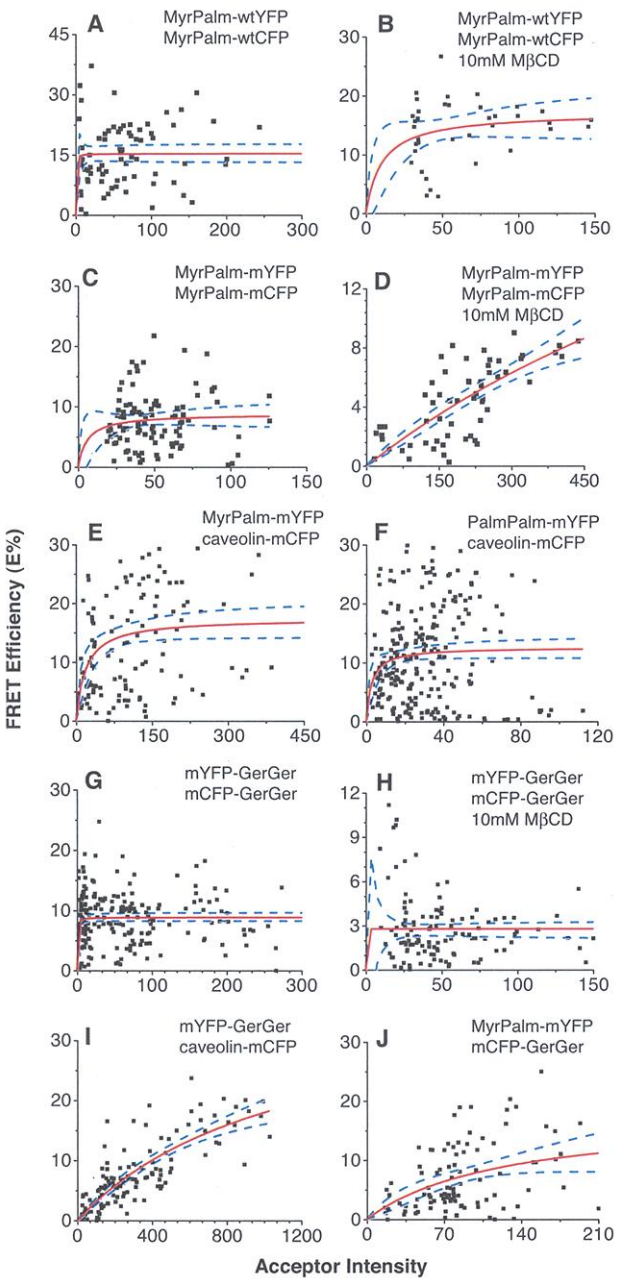

Fig. 3. Determination by FRET of clustering between lipid-anchored fluorescent proteins. The least squares fits of the experimental data (each black square representing one region of interest) to Eq. 1 are shown as red curves, with 95% confidence intervals for the fit shown as flanking blue curves. The fitted value for *K* in Eq. 1 is given for each graph. The *K* values should be compared to the acceptor intensities within the same experiment rather than to *K*'s from other experiments, whose absolute intensity scales are not directly comparable. (**A**) FRET *E*% between MyrPalm-wild-type-CFP and MyrPalm-wild-type-YFP ($K = 0.2 \pm 1.2$). (**B**) MyrPalm-wild-type-CFP and MyrPalm-wild-type-YFP after treatment with 10 mM MβCD ($K = 10 \pm 10$). (**C**) MyrPalm-mCFP and MyrPalm-mYFP (L221K) in untreated cells ($K = 6 \pm 8$). (**D**) MyrPalm-mCFP and MyrPalm-mYFP after MβCD ($K = 1300 \pm 1100$). (**E**) Full-length caveolin-1–mCFP (L221K) and MyrPalm-mYFP L221K ($K = 19 \pm 9$). (**F**) Caveolin-1–mCFP and PalmPalm-mYFP F223R ($K = 3 \pm 2$). (**G** and **H**) mYFP-GerGer and mCFP-GerGer (F223R), (G) before ($K = 0.3 \pm 0.3$) and (H) after 10 mM MβCD ($K = 0.1 \pm 4$). (**I**) mYFP-GerGer and caveolin-1–mCFP F223R ($K = 1100 \pm 300$). (**J**) mCFP-GerGer F223R and MyrPalm-mYFP F223R ($K = 123 \pm 90$).

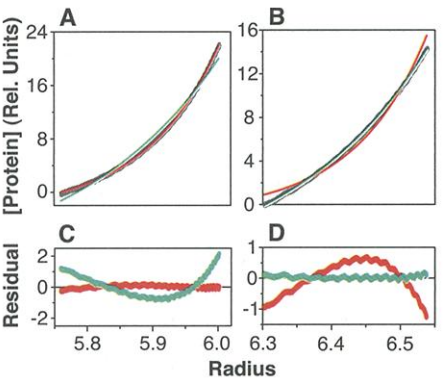

Fig. 4. Sedimentation equilibrium analytical ultracentrifugation of wild-type and monomeric YFP. Sedimentation equilibrium experiments were performed by standard protocol (*15*, *17*). (**A** and **B**) wtYFP (A) and monomeric YFP L221K (B) data sets (gray) were fit globally at multiple speeds and concentrations to the monomeric (green) and dimeric (red) molecular weights. (**C** and **D**) The residual differences between the predicted distribution and the data for wtYFP (C) and mYFP L221K (D). Data shown are for 20,000 rpm at 230 μM.

Table 1: Fluorescence and dissociation of wild-type versus mYFPs without lipid modifications. Dissociation constant K_d (mM) derived from the association constant (K_a) was measured by sedimentation equilibrium analytical ultracentrifugation. Variance (goodness of fit) was determined by global analysis with a nonlinear least-squares algorithm in the software provided by Beckman. Each value is statistically significant.

Mutation	Quantum yield	Extinction coefficient (M^{-1} cm^{-1})	K_d	Variance
Wild type	0.67	67,000	0.11	1.25E-3
L221K	0.67	64,000	9.7	1.35E-3
F223R	0.53	65,000	4.8	1.48E-3
L221K/F223R	0.68	59,000	2.4	4.60E-4
A206K	0.62	79,000	74*	6.65E-4*

*Due to the extreme monomeric nature of this protein it was difficult to determine an accurate dissociation constant for a hypothetical dimer.

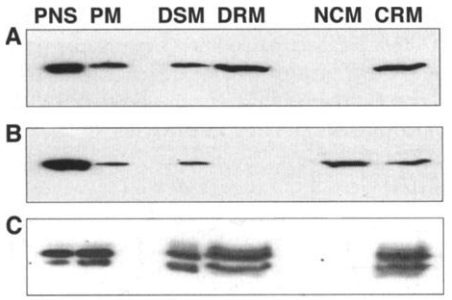

Fig. 5. Fractionation of MDCK plasma membrane reveals differential partitioning of acyl- and prenyl-modified YFP. MyrPalm-mYFP L221K and mYFP-GerGer F223R stably transfected MDCK cells were selected with 200 ng/ml G418 (Gibco). Fractionations were performed as described (*5*, *7*) with the addition of a Percoll gradient to separate plasma membrane (PM) from intracellular membranes in a postnuclear supernatant (PNS) (*22*, *23*) before carbonate or detergent fractionation. One-half of the PM was fractionated with detergent (*5*) and one-half with carbonate (*7*, *24*). Equal volume fractions were collected of detergent-soluble membrane (DSM), detergent-resistant membrane (DRM), noncaveolar membrane (NCM), and caveolae-rich membrane (CRM). (**A**) Western blot with antibody against GFP (Covance) of MyrPalm-mYFP fractions shows enrichment in detergent-insoluble and caveolae-rich fractions. (**B**) Blot by means of antibody against GFP of mYFP-GerGer fractions shows enrichment in detergent-soluble and noncaveolar membranes. (**C**) Immunoblot of endogenous caveolin by antibody against caveolin (Transduction Labs), with partitioning identical to that of the MyrPalm-mYFP.

FRET experiments on live cells. MyrPalm-mYFP (Fig. 5A) partitioned primarily into a detergent-resistant membrane fraction (DRM) and almost exclusively with low-density caveolae-rich membranes (CRM), consistent with the partitioning of endogenous caveolin (Fig. 5C). Conversely, mYFP-GerGer was relatively excluded from DRM and CRM (Fig. 5B) (*7*). These experiments further confirm that lipid modifications alone are sufficient to confer specific sublocalization into or outside of lipid rafts within the plasma membrane.

Our data examining fluorescent proteins attached to the cytosolic side of the plasma membrane complement previous studies using FRET between dye-labeled antibodies, toxins, or ligands to look for clustering of proteins anchored by glycosylphosphatidylinositol (GPI) linkages to the extracellular leaflet of the plasma membrane (*14*, *15*, *20*). Until now, all *Aequorea*-derived GFPs and mutants of any color have contained the hydrophobic patch of Ala^{206}, Leu^{221}, and Phe^{223} responsible for dimerization of the beta barrels. Our new mutations to positively charged residues should prevent dimerization of all colors and are advisable whenever assessing intermolecular interactions of pairs of GFP fusion proteins.

These mutants allowed direct determination in living cells that acylated proteins associate in a manner predicted by models for clustering of proteins into the liquid-ordered phase (*5*). They cluster with each other in lipid rafts and with full-length caveolin-1, a marker for caveolae, suggesting similar lipid compositions and environments in the two structures. Raft disruption with MβCD not only disaggregates acylated fluorescent proteins but also alters numerous signaling events (*15*, *16*, *21*), demonstrating the importance of these domains for cellular function.

References and Notes

1. K. Simons, D. Toomre, *Nature Rev. Mol. Cell. Biol.* **1**, 31 (2000).
2. E. Ikonen, *Curr. Opin. Cell. Biol.* **13**, 470 (2001).
3. C. C. Garner, J. Nash, R. L. Huganir, *Trends Cell. Biol.* **10**, 274 (2000).
4. M. Colledge, J. Scott, *Trends Cell. Biol.* **9**, 216 (1999).
5. K. A. Melkonian, A. G. Ostermeyer, J. Z. Chen, M. G. Roth, D. A. Brown, *J. Biol. Chem.* **274**, 3910 (1999).
6. P. S. Pyenta, D. Holowkà, B. Baird, *Biophys. J.* **80**, 2120 (2001).
7. K. S. Song *et al.*, *J. Biol. Chem.* **271**, 9690 (1996).
8. J. E. Schnitzer, D. P. McIntosh, A. M. Dvorak, J. Liu, P. Oh, *Science* **269**, 1435 (1995).
9. R. Y. Tsien, *Annu. Rev. Biochem.* **67**, 509 (1998)
10. A. Miyawaki, R. Y. Tsien, *Methods Enzymol.* **327**, 472 (2000).
11. M. D. Resh, *Biochim. Biophys. Acta* **1451**, 1 (1999).
12. P. J. Casey, *Science* **268**, 221 (1995).
13. CFP and YFP were enhanced versions ECFP and YFP 10C Q69K (*9*). The signal for geranylgeranylation (GerGer) was a COOH-terminal CLLL from Rho; PalmPalm, an NH_2-terminal MLCCMRRTKQ from Gap43; MyrPalm, an NH_2-terminal MGCIKSKRKDNLNDDE from Lyn kinase. Full-length cDNA of bovine caveolin-1 was fused to the NH_2-terminus of CFP and YFP. Single-letter abbreviations for the amino acid residues are as follows: A, Ala; C, Cys; D, Asp; E, Glu; F, Phe; G, Gly; H, His; I, Ile; K, Lys; L, Leu; M, Met; N, Asn; P, Pro; Q, Gln; R, Arg; S, Ser; T, Thr; V, Val; W, Trp; and Y, Tyr.
14. A. K. Kenworthy, M. Edidin, *J. Cell Biol.* **142**, 69 (1998).
15. Supplementary methods and references are available on *Science* Online at www.sciencemag.org/cgi/content/full/296/5569/913/DC1.
16. L. J. Pike, J. M. Miller, *J. Biol. Chem.* **273**, 22298 (1998).
17. T. M. Laue, W. F. Stafford, *Annu. Rev. Biophys. Biomol. Struct.* **28**, 75 (1999).
18. G. N. Phillips, in *Green Fluorescent Protein: Properties, Applications, and Protocols*. M. Chalfie and S. Kain, Eds. (Wiley-Liss, New York, 1998), pp. 77.
19. F. Yang, L. G. Moss, G. N. Phillips Jr., *Nature Biotechnol.* **14**, 1246 (1996).
20. R. Varma, S. Mayor, *Nature* **394**, 798 (1998).
21. S. Parpal, M. Karlsson, H. Thorn, P. Stralfors, *J. Biol. Chem.* **276**, 9670 (2001).
22. E. J. Smart, Y. S. Ying, C. Mineo, R. G. Anderson, *Proc. Natl. Acad. Sci. U.S.A.* **92**, 10104 (1995).
23. R. D. Lasley, P. Narayan, A. Uittenbogaard, E. J. Smart, *J. Biol. Chem.* **275**, 4417 (2000).
24. V. O. Rybin, X. Xu, M. P. Lisanti, S. F. Steinberg, *J. Biol. Chem.* **275**, 41447 (2000).
25. We thank L. Burns, H. Purkey, and M. Petrassi for help with analytical ultracentrifugation and S. Adams, G. Walkup, R. Wachter, and J. Henley for discussion and suggestions. Supported by NIH grants NS27177 (R.T.), DK54441 (A.N.), 2T32 GM07752 (J.V.), and HHMI.

29 November 2001; accepted 25 February 2002

Large-Scale Transcriptional Activity in Chromosomes 21 and 22

Philipp Kapranov,[1] Simon E. Cawley,[1] Jorg Drenkow,[1] Stefan Bekiranov,[1] Robert L. Strausberg,[2] Stephen P. A. Fodor,[1] Thomas R. Gingeras[1]*

The sequences of the human chromosomes 21 and 22 indicate that there are approximately 770 well-characterized and predicted genes. In this study, empirically derived maps identifying active areas of RNA transcription on these chromosomes have been constructed with the use of cytosolic polyadenylated RNA obtained from 11 human cell lines. Oligonucleotide arrays containing probes spaced on average every 35 base pairs along these chromosomes were used. When compared with the sequence annotations available for these chromosomes, it is noted that as much as an order of magnitude more of the genomic sequence is transcribed than accounted for by the predicted and characterized exons.

Transcriptionally active regions of the human genome have been mapped by a combination of the alignment of cDNA sequences to genomic sequences and the annotation of genome sequences to predict coding regions (*1*–*4*). The goal of this study was to develop an empirical map of the transcriptionally active regions of the human genome at the nucleotide level and to relate this map to the sequence annotations derived from the two general approaches listed above. Previous reports (*5*) have relied on the annotations of the human genome to guide the authors in choosing which genomic regions to evaluate to determine the transcription profile of a cell type (exon arrays). In contrast, we have

[1]Affymetrix, Santa Clara, CA 95051, USA. [2]National Cancer Institute, Bethesda, MD 20892, USA.

*To whom correspondence should be addressed. E-mail: tom_gingeras@affymetrix.com